Construction and Building Materials 453 (2024) 138937

Contents lists available at ScienceDirect

Construction and Building Materials

journal homepage: www.elsevier.com/locate/conbuildmat

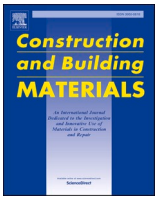

Effect of elevated temperature on the bond behaviour of adhesive shear joints between glass substrate and iron-based shape memory alloy strip

Zhikang Deng [a,*], Vlad-Alexandru Silvestru [a], Lingzhen Li [a,b,c], Elyas Ghafoori [b,d], Andreas Taras [a]

[a] Institute of Structural Engineering, ETH Zurich, Zurich 8093, Switzerland
[b] Empa, Swiss Federal Laboratories for Materials Science and Technology, Dubendorf 8600, Switzerland
[c] Department of Civil and Environmental Engineering, The Hong Kong Polytechnic University, 999077, China
[d] Institute for Steel Construction, Faculty of Civil Engineering and Geodetic Science, Leibniz University Hannover, Hannover 30167, Germany

ARTICLE INFO

Keywords:
Iron-based shape memory alloy (Fe-SMA)
Glass
Epoxy adhesive
Lap-shear joint
Bond behaviour
Debonding
Elevated temperature

ABSTRACT

Glass has been increasingly used as structural elements, such as glass beams or fins. Previous feasibility studies have shown increased initial and post-fracture load-bearing capacity of laminated glass beams post-tensioned with adhesively bonded iron-based shape memory alloy (Fe-SMA) strips. However, the potential elevated service temperatures were not considered, which significantly degraded the material properties of the adhesive. This study experimentally investigated the mechanical behaviour of Fe-SMA-to-glass lap-shear joints with an epoxy adhesive at different temperatures of 23 °C, 50 °C, and 80 °C, representing room temperature and typical elevated service temperatures. The results showed that, compared with the one at room temperature, the load-carrying capacity remained nearly unchanged at 50 °C and decreased by approximately 20 % at 80 °C. On the contrary, the effective bond length increased from approximately 116 mm to 250–300 mm. The failure modes, the tensile strain of the iron-based shape memory alloy, the bond-slip behaviour, and the fracture energy of the joints were also evaluated. The current study fills a significant research gap in the engineering application of strengthening glass structures by bonded pre-stressed Fe-SMA strips. Moreover, the results may also significantly contribute to the future application of the selected adhesive at elevated temperatures.

1. Introduction

Glass has been increasingly applied for structural elements in the last few decades. Examples of such structural glass elements are glass beams [1,2], as shown in Fig. 1a. Brittle failure modes are commonly associated with glass and its inability to redistribute stress concentrations poses a challenge in utilizing glass for structural elements. The initial and post-fracture states should be considered during the design process to comply with safety requirements. Laminated safety glass (LSG) addresses these concerns, however, its residual load-carrying capacity is significantly lower than that before initial glass breakage. Post-tensioned laminated glass beams have been developed as an alternative to address the limitations of laminated glass, as shown in Fig. 1b. The post-tensioned laminated glass beams are still capable of carrying significant loads after crack initiation, and ductile failure modes can be achieved, as shown in Fig. 1c.

Strips made of stainless steel [1,3,4] and fibre-reinforced plastic (FRP) [5,6] have been used for post-tensioning glass beams in previous research, similar to post-tensioning of steel and concrete structures. However, post-tensioning with stainless steel and FRP generally requires complex setups and additional components for anchorage in the case of laminated glass beams.

Shape memory alloys (SMAs) are suitable materials for more efficient pre-stressing procedures due to their shape memory effect (SME). They are capable of undergoing two lattice transformations, exhibiting a unique ability to recover their original shape after the second one. The first transformation occurs through the mechanical pre-straining of the material, while the second transformation is triggered by heating the material to a target temperature followed by cooling naturally to ambient temperature. The shape memory effect allows the generation of compressive pre-stress in the parent structures when SMA elements are fixed to them. Common SMA types, such as Nickel-Titanium (Ni-Ti)-based shape memory alloys and Copper (Cu)-based shape memory alloys, have been used in the past in various fields, such as automotive [7],

* Corresponding author.
E-mail address: deng@ibk.baug.ethz.ch (Z. Deng).

https://doi.org/10.1016/j.conbuildmat.2024.138937
Received 22 July 2024; Received in revised form 3 October 2024; Accepted 25 October 2024
Available online 5 November 2024
0950-0618/© 2024 The Authors. Published by Elsevier Ltd. This is an open access article under the CC BY license (http://creativecommons.org/licenses/by/4.0/).

robotics [8], and aerospace [8]. The iron-based shape memory alloys (Fe-SMAs) [9,10] are more attractive and promising for civil engineering applications due to their lower production costs and excellent mechanical properties [11]. The following Fe-SMA strengthening techniques can be differentiated from previous research and applications:

(i) Near-surface mounting (NSM) technique - part of the original material is removed and Fe-SMA rebars/strips are embedded [12,13];

(ii) Mounting with mechanical anchorage - generally, holes are drilled in the parent structure and the Fe-SMA is fixed with bolts/anchors [14–16];

(iii) Externally bonded (EB) strengthening - adhesively bonding Fe-SMA strips to the surface of structural elements [17,18].

Among these techniques, externally bonded strengthening is deemed most suitable for structural glass components, since no mechanical processing of the glass is necessary and a distributed stress transfer can be achieved.

Recent research [17–19] has demonstrated the potential of adhesive bonding as a suitable alternative for realizing the end anchorage of Fe-SMA strips on glass beams. The basic concept of post-tensioning laminated glass beams by using adhesively bonded Fe-SMAs is shown in Fig. 2. The Fe-SMA strips are firstly pre-strained to a target strain level (ε_{pre}) under tensile force; then, the tensile force is released (unloading), as shown in. Fig. 2a. This step is generally conducted by the Fe-SMA manufacturers or in laboratories. The pre-strained Fe-SMA strips are adhesively bonded to the edges of the glass beam, as shown in step Fig. 2b. After curing of the adhesive, The pre-stress is generated through activation of the Fe-SMA strips, as shown in Fig. 2c, by first heating the Fe-SMA to a target temperature ($T_{activation}$) followed by cooling naturally to ambient temperature ($T_{ambient}$). The Fe-SMA partially transforms from martensite back to austenite during activation and tries to recover to its original length. Due to the bonding of the Fe-SMA strips to the parent structure, a recovery tensile stress (σ_{rec}) in the Fe-SMA and a compressive stress in the glass beam, respectively, are generated during activation. The material behaviour of the Fe-SMA during pre-straining and activation is shown in Fig. 3.

As shown in Fig. 2c, the bonded Fe-SMA strengthening system has two zones: the activation zone (the Fe-SMA strips were heated to the target temperature) and the bonded anchorage zone (at the two ends of the glass bemas, where the Fe-SMA strips were not activated). The activation temperature is applied only to the activation zone to generate prestress. In the current study, we focus primarily on the bonded anchorage zone, where the pre-stressing force is transferred to the glass substrate. Hence, the Fe-SMA strips were not activated, and the activation temperatures were not considered in this investigation.

Adhesives are typically the weakest and most crucial components in adhesively bonded systems. Therefore, the selection of appropriate adhesives is essential for ensuring good performance of the Fe-SMA-to-glass bonded joints. Although various studies exist about the behaviour of different adhesives in glass-metal joints [20–22] and the gained knowledge might be applicable, almost no investigations are available for the structural performance of joints between glass and Fe-SMA strips. To investigate the feasibility of post-tensioning glass elements with adhesively bonded Fe-SMA strips, the mechanical properties and effective bond length of Fe-SMA-to-glass lap-shear joints were investigated experimentally [19]. Following the experimental investigations, a finite element model was developed to evaluate the effect of adhesive thickness, Fe-SMA strip thickness, and bond length on the structural behaviour of Fe-SMA-to-glass lap-shear joints [23]. The feasibility of post-tensioning glass beams with adhesively bonded Fe-SMA strips was investigated experimentally under a four-point bending configuration by Silvestru et al. [17] and Rocha et al. [18]. These investigations were carried out at room temperature. The influence of elevated service temperature on the adhesively bonded joints was not considered. The service temperature will significantly influence the adhesive strength and can't be neglected, according to previous research on FRP/CFRP-to-steel bonded joints [24–26] and FRP-to-concrete bonded joints [27,28]. The service temperature should be lower than the glass transition temperature T_g (at which the material will transit from a relatively brittle or glassy state into a viscous or rubbery state), if possible, to ensure a good bonding performance. Yao et al. [24] conducted an experimental study on FRP-to-steel single lap-shear joints bonded by an epoxy resin structural adhesive under different temperatures. The results showed that the average bond strength increased in the temperature range of 25–50 °C, and decreased significantly from 50 to 100 °C as the glass transition temperature T_g was exceeded. The experimental study by Firmo et al. [29] on double-lap shear tests for concrete blocks strengthened with CFRP strips externally bonded with epoxy adhesive showed that with increased temperature: *(i)* the effective bond length increased; *(ii)* the stiffness and the maximum shear stress suffered considerable reductions; *(iii)* the failure mode changed from cohesive to adhesive; and *(iv)* the overall stiffness and strength of CFRP–concrete interface decreased significantly. Previous investigations on the influence of activation temperature on the bonding performance of joints between Fe-SMA and steel [30], and Fe-SMA and mortar [31,32] showed that heating to 200–260 °C degraded the bonding shear strength and fracture energy. However, the heating time was short and the temperature was high. The elevated service temperature was not considered. Hence, these findings do not apply to adhesively bonded Fe-SMA strips for post-tensioning glass elements at elevated temperatures. The service temperature of the façade materials can be as high as 80 °C according to ETAG 002 [33], which is generally higher than the glass transition temperature T_g of the adhesives used in civil engineering. Hence, it is paramount to understand the possible bonding performance degradation of joints between Fe-SMA and glass due to elevated temperatures.

This study addressed the bond behaviour of lap-shear joints between glass and Fe-SMA with a selected epoxy adhesive (SikaPower®-1277) at

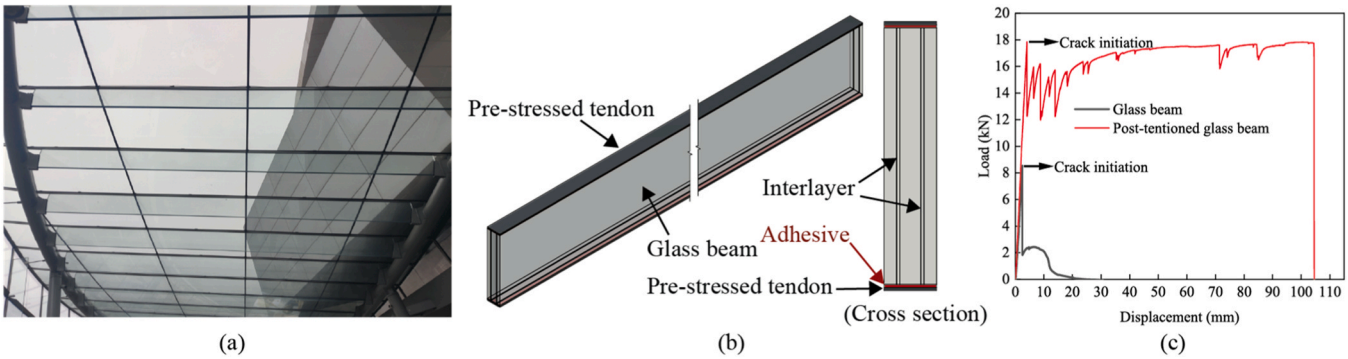

Fig. 1. Application of laminated glass beams as structural elements (a), schematic illustrations of a post-tensioned laminated glass beam (b), and of the achievable improvement in initial and residual load-carrying capacity (c).

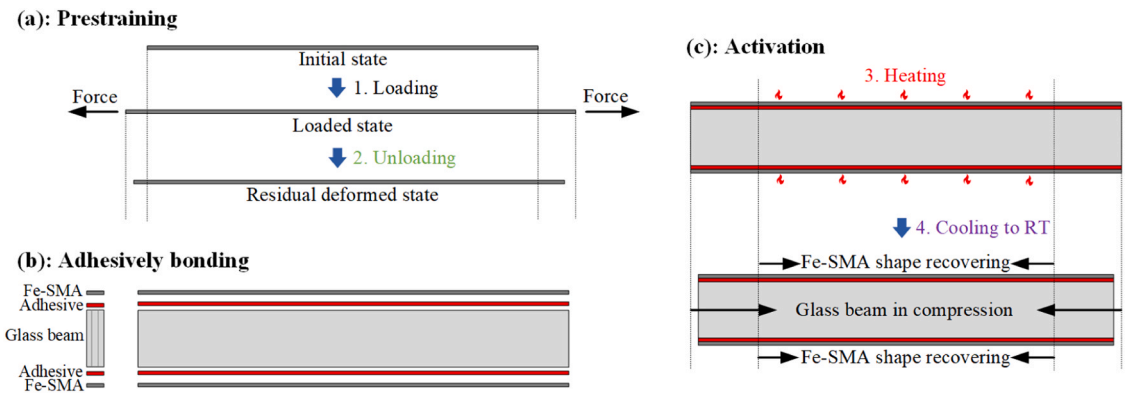

Fig. 2. Production steps for post-tensioning laminated glass beams with adhesively bonded Fe-SMA strips.

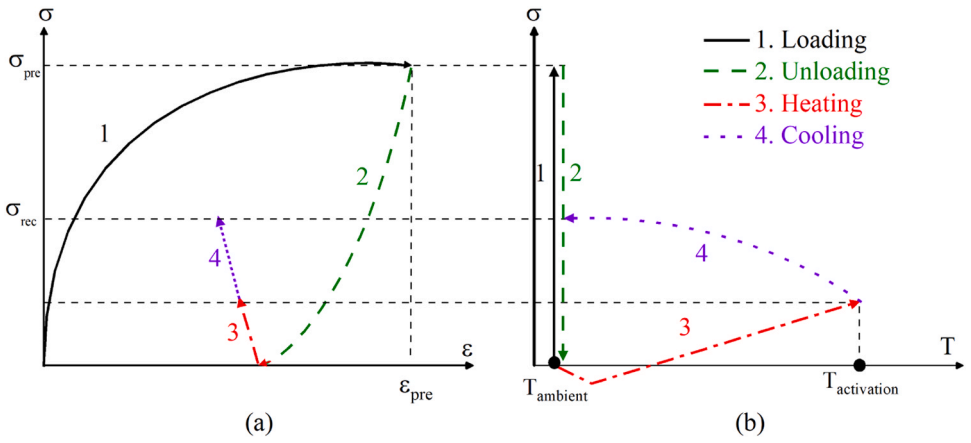

Fig. 3. Qualitative stress versus strain (a) and stress versus temperature (b) relationships of the Fe-SMA during pre-straining and activation.

different temperature levels (23 °C, 50 °C and 80 °C). It expanded upon previous research [17,19,23] by conducting an experimental investigation of Fe-SMA-to-glass adhesively bonded joints. Single lap-shear tests were carried out to study the failure modes, the load-carrying capacity, the tensile strain of Fe-SMA, the bond-slip behaviour, the fracture energy, and the approximate effective bond length. This investigation aimed to explore the short-term performance of the bonded joint at stable service temperature. The effect of temperature cycles and long-term behaviour was not considered in the study.

2. Materials and experimental program

To post-tension glass beams using adhesively bonded Fe-SMA, the adhesive must possess good shear performance to transfer the shear stress when the glass beams are subjected to post-tensioning and bending. Lap-shear tests are widely employed as a common testing method to evaluate the shear performance of adhesive joints. However, previous studies [21,34] using lap-shear tests to examine the bonding of glass to metal substrates used short bond lengths, which are insufficient to represent the strengthening cases with long bond lengths. Therefore, the current study employed a bond length of 450 mm, estimated to be definitely longer than the maximum effective bond length, which is of essential importance for the successful application of post-tensioning structural elements in civil engineering.

2.1. Materials

2.1.1. Glass

Annealed glass was chosen for this investigation. Although fully toughened glass (FTG) and heat-strengthened glass (HSG) have superior strength compared with annealed glass, the latter offers economic advantages. Furthermore, the annealed glass fractures into larger fragments, thereby allowing for a better post-cracking behaviour of laminated glass, especially compared to fully toughened glass. The glass employed in this study has a Young's modulus of 70 GPa and a Poisson's ratio of 0.2. The characteristic tensile bending strength of the glass is 45 MPa, and it exhibits a thermal shock resistance of approximately 40 K, as well as a thermal expansion coefficient of 9E-6 K^{-1}, as specified in EN 572–1 [35]. For the application of adhesively bonded Fe-SMA strips on glass beams, as investigated by [17], the Fe-SMA strips were adhesively bonded to the edges of laminated glass beams. However, in this investigation, the Fe-SMA strips were bonded to the surface of glass panes instead of the edges of laminated glass beams, hence, some effects, such as lower strength at the edge for annealed glass, less bonding surface due to the chamfered glass edges, and partial bonding to the interlayer were out of the scope of this investigation.

2.1.2. Adhesive

The extensive range of structural adhesives available on the market poses a challenge in selecting an appropriate adhesive for this relatively new application. The key criteria that should be considered for bonding Fe-SMA strips to glass are:

(i) Suitability for application on both glass and Fe-SMA;
(ii) Relatively high shear strength and stiffness;
(iii) A notable capacity to withstand varying temperatures up to 80 °C.

In this investigation, the commercially available adhesive SikaPower®-1277 was selected based on its proven good performance in lap-shear joints between glass and Fe-SMA [19,23], as well as in post-tensioned glass beams with adhesively bonded Fe-SMA strips [17].

SikaPower®-1277 is a two-component epoxy which has shown good bonding performance on glass [19], Fe-SMA [36], and steel [37]. The selected basic material properties of SikaPower®-1277 are shown in Table 1. According to the data in [38], the lap-shear strength and the elastic modulus decrease significantly when the temperature increases from 23 °C to 80 °C.

2.1.3. Iron-based shape memory alloy

The Fe-17Mn-5Si-10Cr-4Ni-1(V, C) (mass%) alloy used in this research was developed for the construction industry and is currently produced by re-fer-AG. The basic material properties of the Fe-SMA alloy were investigated in previous research [39] and are presented in Table 2.

For this investigation, the Fe-SMA strips were pre-strained by 2.5 % followed by unloading. Residual strain is obtained due to phase transformation and plastic deformation. The residual strain due to phase transformation can be recovered partially when the Fe-SMA is heated to a target temperature. After pre-straining, the pre-strained Fe-SMA strips with a thickness of 1.5 mm were cut into dimensions of 780 mm (length) × 25 mm (width) using a Schechtl MSC Shear cutting machine.

2.2. Test specimens

A series of lap-shear tests were conducted at three different temperatures (23 °C, 50 °C, and 80 °C). The room temperature of 23 °C was considered as the reference temperature. The temperature of 80 °C was selected as the maximum temperature that can be reached in a transparent facade according to ETAG 002 [33], while 50 °C was selected as an intermediate value to reveal more details. A total of ten specimens were tested, as shown in Table 3. Three tests were conducted at each temperature, and one (LS-00-Calibration) was used for temperature calibration.

The digital image correlation (DIC) technique was used to measure displacement and strain for later analysis of the shear behaviour at 23 °C and 50 °C. As the DIC was not applicable at 80 °C because the climate chamber has to be closed during the test to maintain stable test temperatures, a Linear Variable Displacement Transducer (LVDT) was used to measure the slip, and strain gauges were used to measure the strains on the glass for the tests conducted at this temperature.

The glass dimensions were 500 mm×250 mm x 10 mm (length x width x thickness), and the adhesive layer was controlled at approximately 1.5 mm in thickness, which was defined in previous research [19]. A long bond length of 450 mm was designed to allow analyzing the maximum effective bond length, as shown in Fig. 4.

To ensure good bonding quality, both the glass plates and Fe-SMA strips underwent careful surface preparation before bonding. They were first cleaned with acetone to eliminate any surface contaminants, such as grease or dust. The Fe-SMA surfaces were then sandblasted at a pressure of 8 bar using 0.15–0.21 mm aluminium oxide to remove the oxidized layer and increase the surface roughness. After sandblasting, the Fe-SMA surfaces were cleaned again with acetone before the adhesive was applied. After surface preparation, the two-component adhesive was mixed and applied to the glass and Fe-SMA bond areas according to the manufacturer's guidelines. To control the bond length, 1.5 mm-thick Teflon strips were placed between the Fe-SMA strip and the glass plate at the two ends of the bond line at a distance of 450 mm.

Table 1
Selected information for SikaPower®-1277 [38].

Elastic modulus (MPa)		Lap-shear strength (MPa)		Elongation at break (%)		Glass transition temperature (°C)	Mixing ratio (by volume)
23 °C	80 °C	23 °C	80 °C	23 °C	80 °C		
1940	138	28	13	7.4	17	approx. 67	2:1

Table 2
Material properties of pre-strained (2.5 %) Fe-SMA [39].

Young's modulus (MPa)	Ultimate tensile strength (MPa)	Strain at ultimate tensile strength (%)	0.2 % yield strength (MPa)
168,909	953.04	29.06	491.47

Table 3
Overview of the investigated Fe-SMA-to-glass lap-shear test specimens.

Specimens ID	Test temperature	Slip and strain measurement
LS−00-Calibration	50 °C, 80 °C	-
LS−01-(23 °C), LS−02-(23 °C), LS−03-(23 °C)	23 °C	DIC
LS−04-(50 °C), LS−05-(50 °C), LS−06-(50 °C)	50 °C	DIC
LS−07-(80 °C), LS−08-(80 °C), LS−09-(80 °C)	80 °C	LVDT and strain gauges

After bonding, steel weights were put on the top surface of the Fe-SMA to squeeze out excessive adhesive and ensure an even bond thickness. They were removed after 24 hours, and the specimens were then stored in the climate room at 23 °C and 50 % relative humidity for at least 14 days. Fig. 5 illustrates the specimen preparation process. One specimen after adhesive bonding is shown in Fig. 6.

2.3. Test setup and test procedure

The test setup, depicted in Fig. 7a, was carefully designed for the lap-shear tests on Fe-SMA-to-glass joints, to ensure a minimum eccentric loading and restrict the out-of-plane deformation of specimens. The glass panels were fixed on a rigid, 27.0 mm thick steel plate with two 15.0 mm thick steel bars to restrict the out-of-plane movement of the glass panels. The steel grade of these parts was S355J2+N. The tests were conducted within a climate chamber (Zwick, W91118) to ensure a relatively stable temperature throughout the testing. The setup was installed in a vertical position on the Zwick universal testing machine (with a load capacity of 200 kN). At its top, the support steel frame was connected with a hinge that allowed rotations around the z-axis. At the bottom, the Fe-SMA strip was mechanically clamped to the Zwick machine. A sketch of the specimen fixed in the climate chamber is shown in Fig. 7b.

The tests were conducted under a displacement-controlled loading scheme at a displacement rate of 0.02 mm/s to allow for stable crack initiation and propagation. The clamped Fe-SMA strip was pulled downwards in a vertical direction, as shown in Fig. 7b, until specimen failure, i.e., debonding, Fe-SMA rupture, or glass panel fracture.

The specimens were first installed in the climate chamber and heated to the desired temperatures of 50 °C and 80 °C, respectively, with the chamber closed. For the tests at 50 °C, the chamber was opened once the target temperature was reached, and then the climate chamber was kept running to compensate for energy loss. In the meantime, the temperature of the specimens was measured using thermocouples. In this case, the DIC was used to measure the strain field with the open climate chamber door.

2.4. Measurement instrumentation

Before conducting the lap-shear tests, temperature calibration tests were carried out to determine the heating and temperature monitoring strategies. To achieve this, 18 thermocouples (TC1-TC18) were installed on the specimen, with six of them (TC1-TC6) on the Fe-SMA strip, six (TC7-TC12) in the adhesive, and six (TC13-TC18) on the glass surface, respectively, as shown in Fig. 8. By identifying the temperature development at different points on the specimen, a limited number of

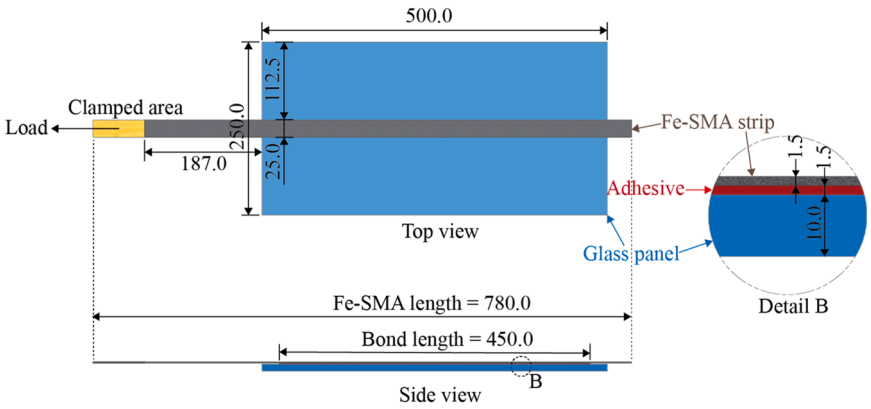

Fig. 4. Dimensions of the lap-shear specimens in [mm].

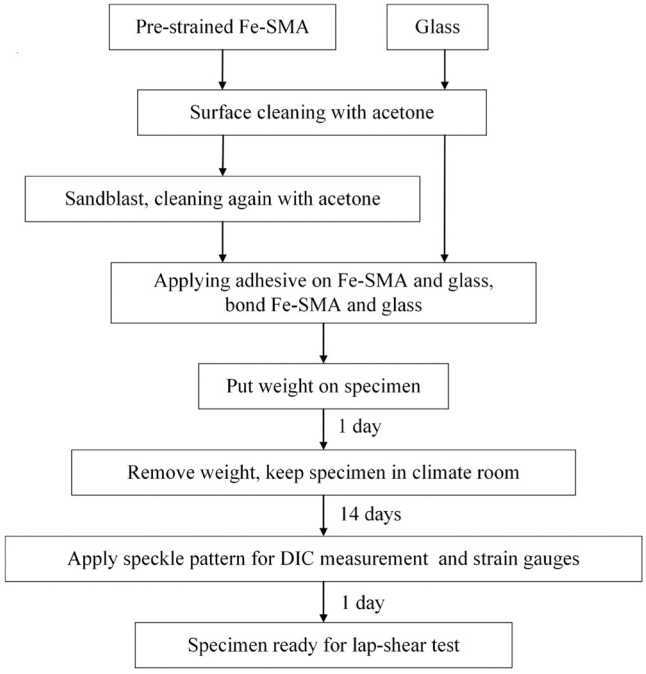

Fig. 5. Manufacturing steps for the lap-shear test specimens.

thermocouples could be used for the rest of the tests to monitor the temperature of the specimens. This allowed, on the one hand, to avoid the need to install numerous thermocouples on each test specimen, and, on the other hand, to prevent the installation of thermocouples in the adhesive layers, avoiding to artificially damage the adhesive bond. The thermocouples TC13 and TC18 were used to monitor the temperatures for all the lap-shear test specimens. They were installed on the glass near the bond front and end, as shown in Fig. 8.

Strain gauges were employed to measure the strain on the Fe-SMA strip for the tests at 80 °C. A digital image correlation (DIC) system was employed to measure the strain on both the Fe-SMA strip and on the glass surfaces during the tests at 23 °C and 50 °C. The DIC system was used for the tests conducted at 23 °C and 50 °C since a relatively stable temperature could be maintained with the climate chamber open. The setup configuration for the tests is shown in Fig. 9. DIC measurements were preferred for the tests at 23 °C and 50 °C for two reasons. First, DIC allows measuring large strains and the deformation of Fe-SMA can be as high as 12 %-14 %, according to previous investigations [19], which exceeds the limits of standard strain gauges (up to 3 %-5 %). Second, DIC allows full-field displacement and strain measurements with sufficient precision, enabling the analysis over entire areas of interest compared to punctual analysis enabled by strain gauges. The DIC system was placed in front of the specimen during the lap-shear tests, as shown in Fig. 9a. For the DIC measurements, a white flat paint and a black speckle pattern with a dot size of 0.33 mm were applied with a roller on the top surfaces of the glass and the Fe-SMA strip as shown in Fig. 9b. The DIC measurements were carried out with a VIC-3D 9 system from Correlated Solutions, Inc. Two FLIR 12.3 MP cameras with lenses having a focal length of 24 mm were utilized.

However, to maintain a stable temperature for specimens tested at 80 °C, the climate chamber door needed to remain closed. The DIC system could not be used during the tests at 80 °C in this case. Therefore, strain gauges were applied on these specimens to measure the strains on the Fe-SMA strips. Linear Variable Displacement Transducers (LVDT) were applied to measure the slip at the bond front for the tests at 80 °C. The base of the LVDT was fixed on the glass, and the core extension contacted the support fixed on the Fe-SMA, as shown in Fig. 9c.

Ten strain gauges (SG01-SG10) were installed on the Fe-SMA top surface. The measured values by strain gauges were used to calculate the approximate effective bond length for the tests conducted at 80 °C. The idea was that the bonding zone between zero strain and maximum strain was the active shear zone, which reflected the effective bond length. Strain gauges of type YHFLA-5 that can measure up to 30 %-40 % strain were used. The strain gauges were installed from the bond front (near the loading end) towards the bond end with an interval distance of 50 mm, as illustrated in Fig. 10.

2.5. *Post-processing methods*

The directly obtained experimental data during the tests were *(i)* the load and the displacement measured by the Zwick machine for all specimens, *(ii)* full-field strain/displacement measurements by DIC for the specimens tested at 23 °C and 50 °C, *(iii)* the strain of the Fe-SMA strip measured by strain gauges for specimens tested at 80 °C, and *(iv)* the slip measured by LVDTs for specimens tested at 80 °C. These data were used to analyze the full-range behaviour of the Fe-SMA-to-glass shear joints at different temperatures.

2.5.1. *Tensile strain of glass and Fe-SMA*

For the tests at 23 °C and 50 °C, the DIC data was post-processed to calculate the full-field displacement and strain. This was conducted in the software VIC-3D 9 with a subset size of 21, a step size of 10, and a filter size of 15. A grid of nodes was defined within the area of interest (AOI), as shown in Fig. 11a. The displacements and strains of these nodes were extracted to characterize the behaviour of the Fe-SMA and glass during the tests. Before the evaluation, a coordinate system was set with the origin at the middle of the bond front, as shown in Fig. 11a. The x-axis was defined along the bond line from the origin towards the fixed end of the specimens. The y-axis is parallel to the top surface of the Fe-

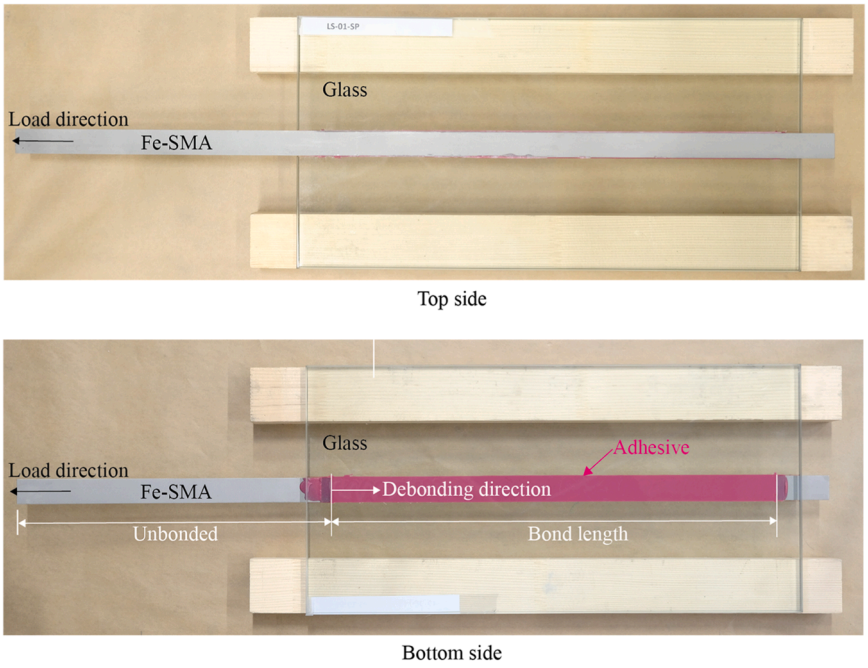

Fig. 6. Lap-shear test specimen after manufacturing.

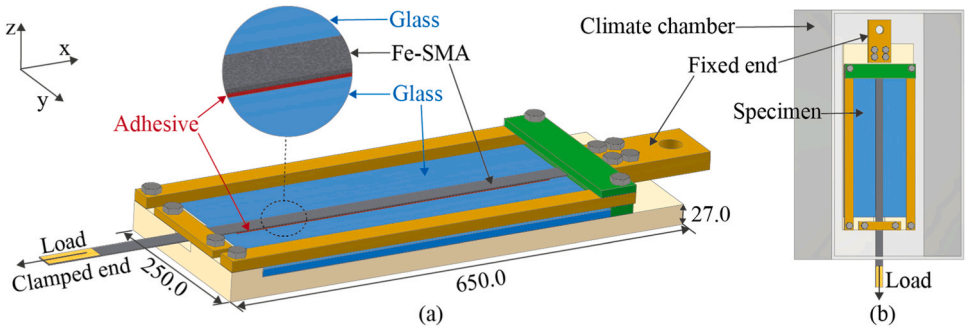

Fig. 7. Detailed test setup with the specimen (a), lap-shear test setup configuration in the climate chamber (b) – provided dimensions in [mm].

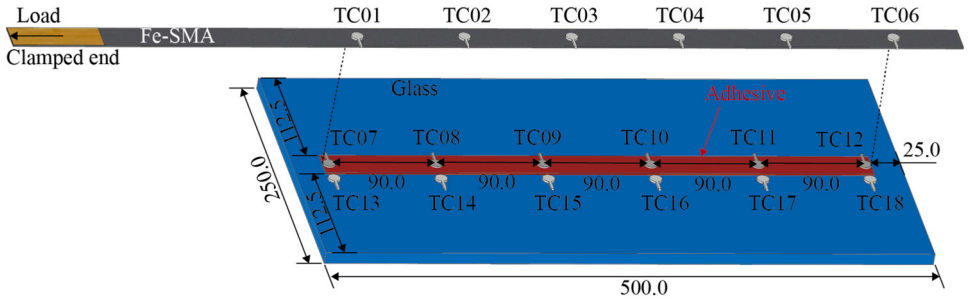

Fig. 8. Positions and numbers of thermocouples used in the temperature calibration test (dimensions in [mm]).

SMA strip and perpendicular to the x-axis. Five rows of nodes (225 nodes with a distance of 2 mm to each other for each row) were defined within the area of interest (AOI). Three rows were defined on the top surface of the Fe-SMA strip, and the other two were on the top surface of the glass panel with a distance of 25.0 mm to the x-axis. This post-processing was based on the assumption that the tensile strains were uniform across the width of the Fe-SMA strips as the values obtained from the DIC measurements did not vary significantly across the width.

2.5.2. *Tensile stress in Fe-SMA strips*

After obtaining the tensile strain on the Fe-SMA strip, the corresponding tensile stress σ_i in the Fe-SMA could be computed by the constitutive relationship (stress-strain relationship) for Fe-SMA under uniaxial tensile loading. The uniaxial tensile stress-strain relationship was calculated based on the two-stage Ramberg-Osgood model [39], which allowed determining more stress-strain data pairs compared with the limited number of data pairs obtained from uniaxial tensile tests.

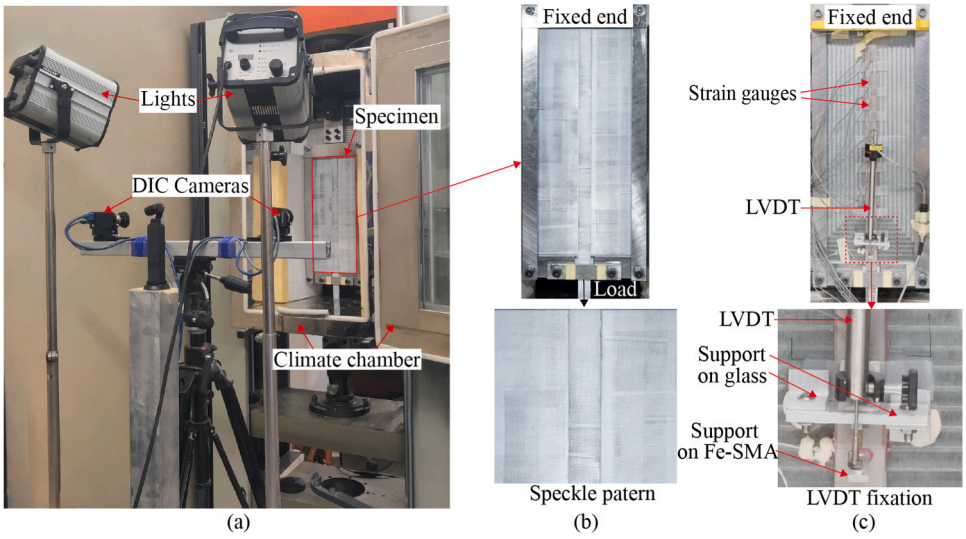

Fig. 9. Test setup with specimen installed in the climate chamber (a), specimen configuration for the tests at 23 °C and 50 °C (b), specimen configuration for the tests at 80 °C (c).

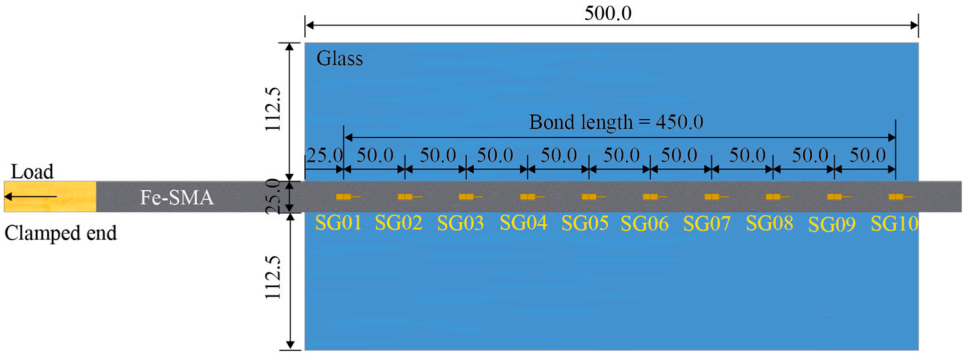

Fig. 10. Positions and numbers of strain gauges for the lap-shear specimens tested at 80 °C [mm].

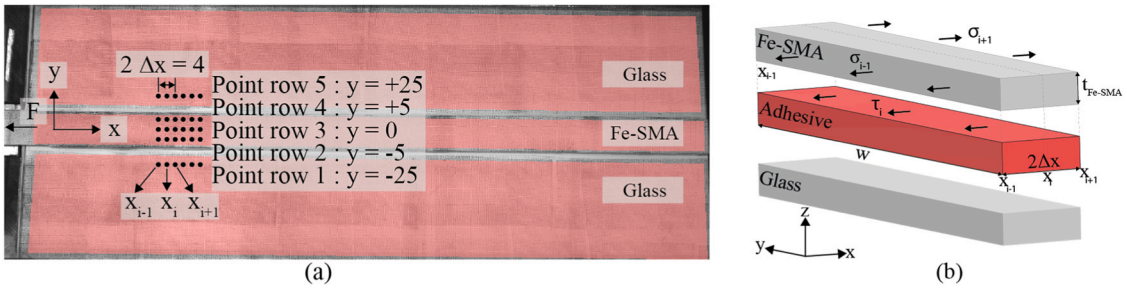

Fig. 11. Schematic view of the nodes used for processing the DIC measurements (a), equilibrium of stresses in a representative infinitesimal part of the joint (b) – provided dimensions in [mm].

2.5.3. *Load-displacement behaviour and load-slip behaviour*

The load-displacement curves were obtained from the Zwick machine. However, the displacement included the deformation of the unboned Fe-SMA as visible in Fig. 6. The main objective of this research was to investigate the bonded part (450 mm of bond line). The displacement of the unbonded Fe-SMA needed to be excluded from the total displacement of the tests, such that the analyzed load-slip curve only reflected the behaviour of the adhesively bonded joint. For the tests at 23 °C and 50 °C, the slip δ_i (the relative displacement between the Fe-SMA strip and the glass panel) at the loaded end of the joint was calculated using Eq. (1). The displacements of the Fe-SMA strip ($U_{2,i}$, $U_{3,i}$, $U_{4,i}$) and the glass panel ($U_{1,i}$ and $U_{5,i}$) were characterized by the displacements of the nodes of rows 2–4, and 1 and 5, respectively, as shown in Fig. 11a. The calculated slip δ_i was used to characterize the slip behaviour of the joints.

$$\delta_i = (U_{2,i} + U_{3,i} + U_{4,i})/3 - (U_{1,i} + \quad U_{5,i})/2 \tag{1}$$

For the tests conducted at 80 °C, the slip at the loaded end of the joint was measured by LVDT.

2.5.4. *Shear behaviour of the adhesive*

An infinitesimal element of the joints, shown in Fig. 11b, was used to calculate the shear stress in the adhesive. Here, w = 25 mm and t_{Fe-SMA} = 1.5 mm were the width and the thickness of the Fe-SMA, respectively.

x_i was the x-coordinate of the points and σ_i was the corresponding tensile stress in the Fe-SMA cross-section.

The equilibrium for the represented infinitesimal Fe-SMA part is shown in Eq.(2). The shear stress τ_i in the cross-section of the adhesive along the x-axis was calculated with Eq.(3).

$$\sigma_{i-1}\cdot w\cdot t_{Fe-SMA} + \tau_i\cdot 2\cdot\Delta x\cdot w = \sigma_{i+1}\cdot w\cdot t_{Fe-SMA} \quad (2)$$

$$\tau_i = \frac{\sigma_{i-1} - \sigma_{i+1}}{2\cdot\triangle x}\cdot t_{Fe-SMA} \quad (3)$$

By correlating the shear stress τ_i and the slip δ_i in the bond length over time, the bond-slip behaviour was obtained. The nodes at the bond front were chosen for the analysis of bond-slip behaviour in this investigation.

2.5.5. Effective bond length

The effective bond length is the active length of the bond line, over which shear stress is transferred between the glass panel and the Fe-SMA strip through the adhesive. It is essential for defining the safe anchorage length in the adhesively bonded joints. The effective bond length of the Fe-SMA-to-glass joints was quantified by the gradient zone of the tensile strain on the Fe-SMA strip (length over which the strain in the Fe-SMA strip drops from a relatively constant value to zero), which corresponds to the length of non-zero shear stress in the adhesive along the bond line (see also evaluation in [19]).

3. Results and discussion

This section presents and discusses *(i)* the temperature calibration test results, *(ii)* the failure modes, *(iii)* the load-displacement behaviour, *(iv)* the load-slip behaviour, *(v)* the tensile strain of the Fe-SMA, *(vi)* the effective bond length, *(vii)* the bond-slip behaviour, and the *(viii)* fracture energy obtained for the specimens tested at different temperatures.

3.1. Temperature calibration test

The temperature calibration tests were carried out to investigate the temperature development at different locations on the specimens. For the temperature calibration test at 50 °C, the temperatures of Fe-SMA, adhesive, and glass are shown in Fig. 12a, Fig. 12c, and Fig. 12e, respectively. The curves indicated that temperature differences between glass, Fe-SMA, and adhesive were relatively small (<2.5 °C). The first drop and kinks of the curves were due to the opening and closing of the climate chamber door. The later kinks were due to adjusting the target temperature of the climate chamber. For the temperature calibration test at 80 °C, the temperatures of Fe-SMA, adhesive, and glass are shown in Fig. 12b, Fig. 12d, and Fig. 12f, respectively. The results indicated that the temperate of glass, Fe-SMA, and adhesive were constant and stable at approximately 80 °C (±0.5 °C). Based on these temperature calibration results, the temperature of the other specimens could be monitored using only two thermocouples, TC13 and TC18, during the tests.

3.2. Failure modes

Four different failure modes were observed during the tests at different temperatures:

(a) Cohesive failure (also called cohesion failure in some literature [36]), where cracks were initiated and propagated in the adhesive layer;

(b) Fe-SMA strip rupture;

(c) Adhesive failure (also called adhesion failure [36]), where failures were initiated in the glass-adhesive interface;

(d) Glass failure, where the glass panel fractured, while the adhesive still bonded the Fe-SMA strip and fractured glass panel.

The observed failure modes of the lap-shear tests are shown in Fig. 13. The failure modes for the tests at 23 °C were mainly cohesive failures, as shown in Fig. 13 (a and b). When the temperature increased, the failure modes were more likely to be adhesive failure, due to the decreased bond strength between the glass and the adhesive, as shown in Fig. 13 (d-e, and g-i). This conclusion was similar to the one obtained from the experimental study on FRP-to-steel single lap-shear joints bonded by epoxy resin structural adhesive presented in [24].

The glass failure shown in Fig. 13 (b, e, and g-i) was due to the dynamic impact at the end phase of crack propagation. They were not considered as glass failure in this case, since a considerable amount of cohesive failure or adhesive failure occurred before glass failure. The glass failure in the case of specimen LS-06–50 °C might be because of defects during manufacturing or damage during transportation of glass. The rupture of the Fe-SMA strip in the case of specimen LS-03–23 °C might have been the result of a loading eccentricity or of a local defect of the Fe-SMA strip.

The following can be summarized from the testing results. With the proper surface preparation, the Fe-SMA-adhesive and glass-adhesive interfaces were stronger than the adhesive, resulting in cohesive failures at room temperature. As the temperature increased, the strengths of the adhesive and of the interfaces were reduced, with evidence being the reduced bond capacities, which will be presented in Section 3.3. However, the strength reduction of the interfaces was more severe than that of the adhesive. Thus, adhesive failure was the major failure mode at 50 °C and 80 °C.

3.3. Load-displacement behaviour

The load-displacement curves for the tests at 23 °C, 50 °C, and 80 °C are shown in Fig. 14a. All the specimens showed ductile failure modes, allowing for observation of crack propagation, except for one specimen (LS-03–23 °C), which failed due to Fe-SMA rupture, and one specimen (LS-06–50 °C), which exhibited glass failure during the test. Table 4 presents the crack initiation loads and maximum loads of all specimens, where the crack initiation loads were defined as the points on the load-displacement curves with a mild drop of tensile load. The mean values of crack initiation loads for the tested specimens at 23 °C, 50 °C, and 80 °C were 32.5 kN, 29.9 kN, and 26.7 kN, respectively. These crack initiation loads were nearly identical to the maximum loads at each of the temperatures, which were 33.3 kN at 23 °C, 30.5 kN at 50 °C, and 26.7 kN at 80 °C. In addition, Table 4 provides values for the maximum tensile stress in the Fe-SMA strips, and for the effective bond length, which will be discussed in Section 3.5.

The load-carrying capacity only decreased slightly (8.4 %) when the test temperature was 50 °C, compared with that at 23 °C, despite the elastic modulus and the strength of the adhesive at 50 °C were much lower compared to those at 23 °C according to the additional product information of SikaPower®-1277 [38]. However, the main reason was that the decreased elastic modulus enabled a longer effective bond length of the joints at 50 °C. When the test temperature was 80 °C, the load-carrying capacity decreased by around 19.8 % compared with that at 23 °C. This was because the test temperature of 80 °C was higher than the glass transition temperature of the adhesive and the adhesive properties degraded more severely.

3.4. Load-slip behaviour

The load-slip curves were obtained using the methods described in Section 2.5.3 and are shown in Fig. 14b. The load-slip behaviour was obtained by DIC measurements for the tests at 23 °C and 50 °C, and by LVDT measurements for the tests at 80 °C. The load-slip curves were similar for the tests at 23 °C and 50 °C, which was in agreement with the similar load-displacement curves for these temperatures shown in Fig. 14a. The tests at 80 °C showed significantly less slip compared with those at 23 °C and 50 °C. One reason was the lower maximum load reached in the tests at 80 °C compared with those at 23 °C and 50 °C. This resulted in less deformation of the Fe-SMA strips. The other reason was that the effective bond length at 80 °C was longer than those at 23

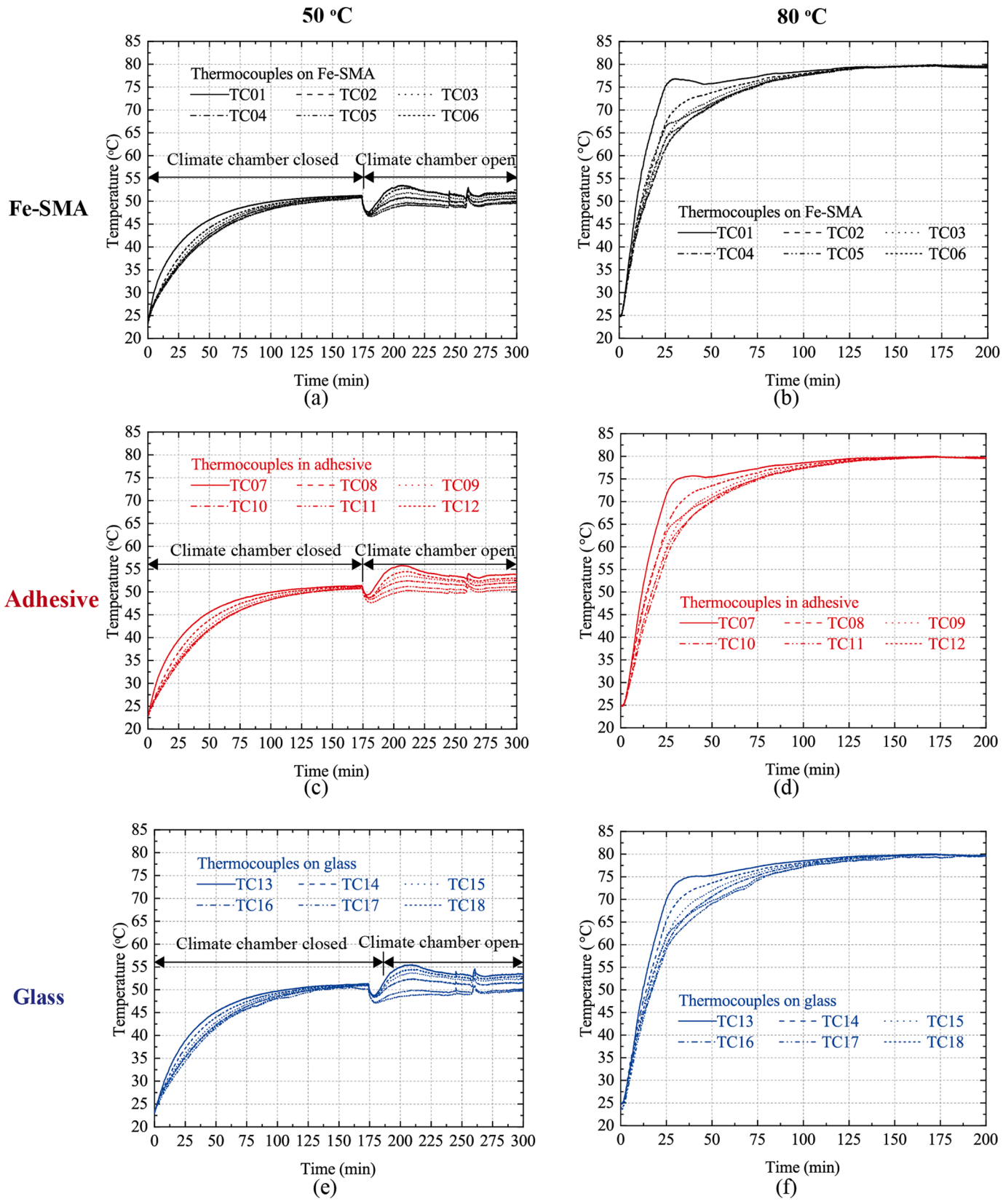

Fig. 12. Temperature on Fe-SMA strip (a), in adhesive (c), and on glass panel (e) during the temperature calibration tests at 50 °C, and temperature on Fe-SMA strip (b), in adhesive (d), and on glass panel (f) during the temperature calibration test at 80 °C.

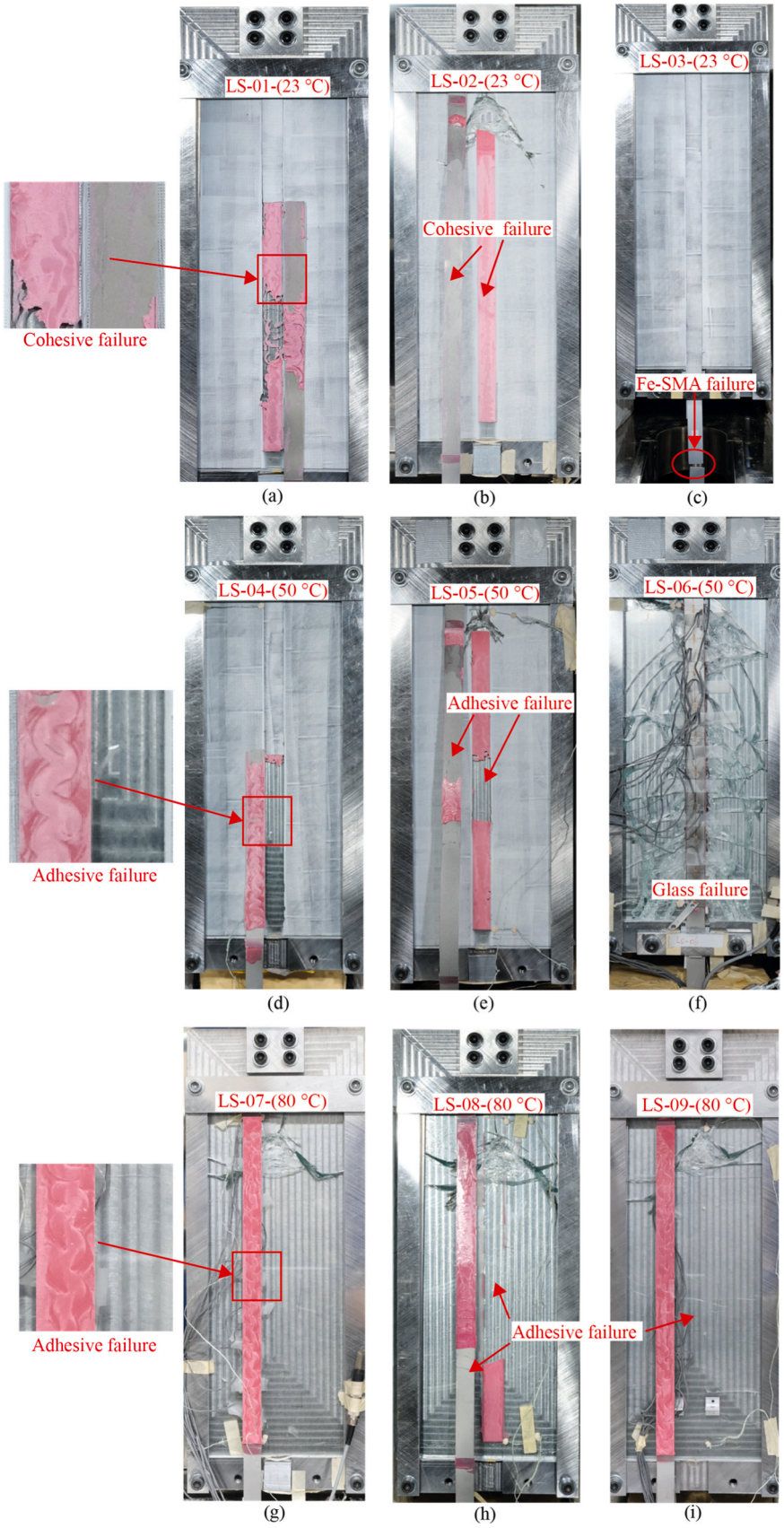

Fig. 13. Fe-SMA-to-glass lap-shear joints failure modes at 23 °C (a-c), 50 °C (d-f) and 80 °C (g-i).

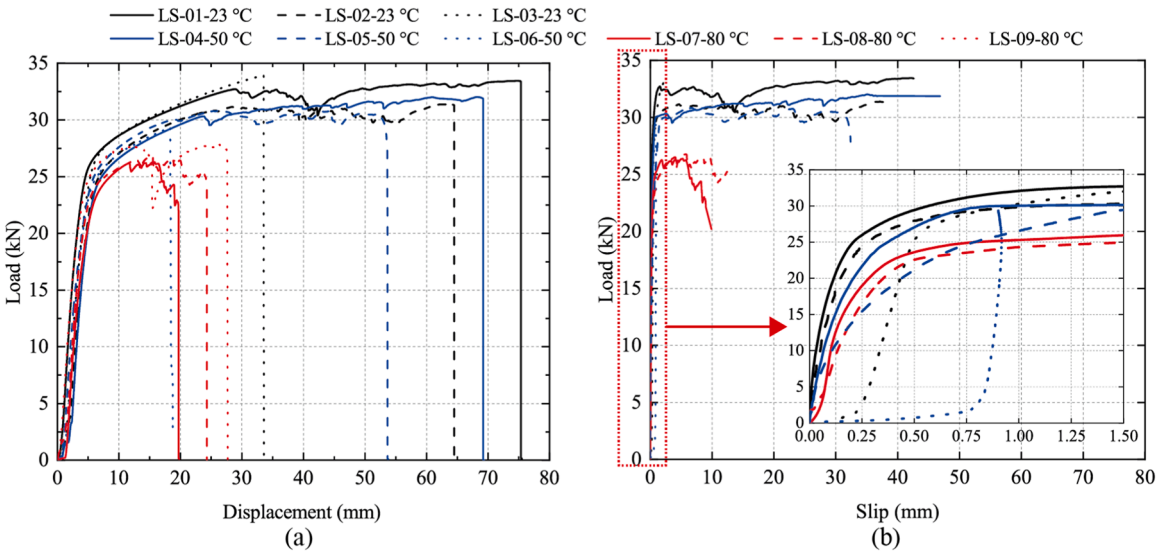

Fig. 14. Load-displacement curves (a), and load-slip curves (b) at 23 °C, 50 °C and 80 °C.

Table 4
Selected mechanical properties determined as mean values and coefficients of variation (CV) based on the single-lap-shear tests at 23 °C, 50 °C and 80 °C.

Properties	23 °C		50 °C		80 °C	
	Mean value	CV	Mean value	CV	Mean value	CV
Crack initiation load (kN)	32.5	3.7 %	29.9	1.4 %	26.7	2.4 %
Maximum load (kN)	33.3	3.4 %	30.5	3.7 %	26.7	2.3 %
Max. tensile stress in Fe-SMA (MPa)	888.9	3.4 %	813.3	3.7 %	712.0	2.3 %
Effective bond length (mm)	116		200		250–300	

°C and 50 °C, which also led to shorter Fe-SMA strip parts that could freely deform before the total debonding. A close-up of the loading stage in Fig. 14b shows that the stiffness of the joints slightly decreased with the increasing temperature. Results for LS-09–80 °C are not shown in Fig. 14b due to the accidental detachment of the LVDT during the test.

The maximum tensile stresses in the Fe-SMA were calculated by dividing the maximum load by the area of the cross-section of the Fe-SMA strip. They are shown in Table 4. It can be seen that the maximum tensile stress in the Fe-SMA strip was below the ultimate tensile strength (953.04 MPa) of Fe-SMA. This means that a higher load-carrying capacity of the joint would be possible with a more robust adhesive.

The mechanical behaviour of the adhesive joints between glass and Fe-SMA included two stages divided by the moment of crack initiation: the load-increasing stage and the crack propagation stage. During the load-increasing stage, the stiffness of the bonded joints exhibited temperature-dependent variations. An increase in temperature resulted in a decrease in joint stiffness, as shown in Fig. 14b. This phenomenon was primarily attributed to the fact that the Young's modulus of the adhesive significantly decreased with rising temperatures [38]. In the crack propagation stage, the results from the tests conducted at different temperatures in this study consistently demonstrated stable crack propagation, regardless of cohesive or adhesive failure. This suggested a ductile failure mode for these types of joints.

3.5. Tensile strain of the Fe-SMA and effective bond length

For the tests at 23 °C and 50 °C, the tensile strain of the Fe-SMA was determined from the DIC measurements. The results are shown in Fig. 15a and Fig. 15b for a representative test specimen at each of the two temperatures. The maximum strains in the Fe-SMA for the tests at 23 °C and 50 °C were around 10.6 % and 9.8 % on average, respectively. Based on the tensile strain of the Fe-SMA, the effective bond length of Fe-SMA-to-glass lap-shear joints was defined for 23 °C and 50 °C, respectively. Effective bond lengths of approximately 116 mm (average of LS-01–23 °C and LS-02–23 °C) at 23 °C and 200 mm (average of LS-04–50 °C and LS-05–50 °C) at 50 °C were determined according to the length of the Fe-SMA strips over which the tensile strains dropped from the maximum values to zero, as shown in Fig. 15a and Fig. 15b. The results at 23 °C were similar to the effective bond length of 120 mm estimated from lap-shear tests on Fe-SMA-to-glass joints in [19]. For the tests at 80 °C, the effective bond length was estimated based on strain gauge measurements instead of DIC measurements. Six strain gauges measured tensile strain before crack initiation for both LS-07–80 °C and LS-08–80 °C, as shown in Fig. 15c. Since the strain gauges were installed with an internal distance of 50 mm as shown in Fig. 10, the effective bond length at 80 °C was estimated between 250 mm and 300 mm. The strain gauge values were also plotted along the bond line, as shown in Fig. 15d, as a similar way to Fig. 15a and b. Since strain gauges were installed with an internal distance of 50 mm, the strain values between the strain gauges were unsure. The effective bond length was estimated to be between 250 mm and 300 mm, which was not as accurate as the results obtained based on the DIC measurements.

As the temperature increased, the effective bond length likewise increased. This phenomenon can be attributed to a decrease in the adhesive's stiffness, leading to larger deformation of the adhesive. Consequently, longer bond lengths were subjected to shear stress.

3.6. Bond-slip behaviour and fracture energy

The triangular bond-slip behaviours from representative tests at 23 °C and 50 °C are shown in Fig. 16a and Fig. 16b. Since DIC was not used during the tests at 80 °C, the bond-slip behaviours at 80 °C were calculated directly from the load-slip curves using an analytical model given by [40], and the results are shown in Fig. 16c. This analytical model [40] involved a mapping between the external load and dissipated fracture energy, whose derivative is the shear stress in the bond-slip behaviour.

The triangular bond-slip behaviours contain an ascending branch, which indicates the shear stiffness of the joints. The descending branch shows the damage evolution. The area under the bond-slip curve, shown

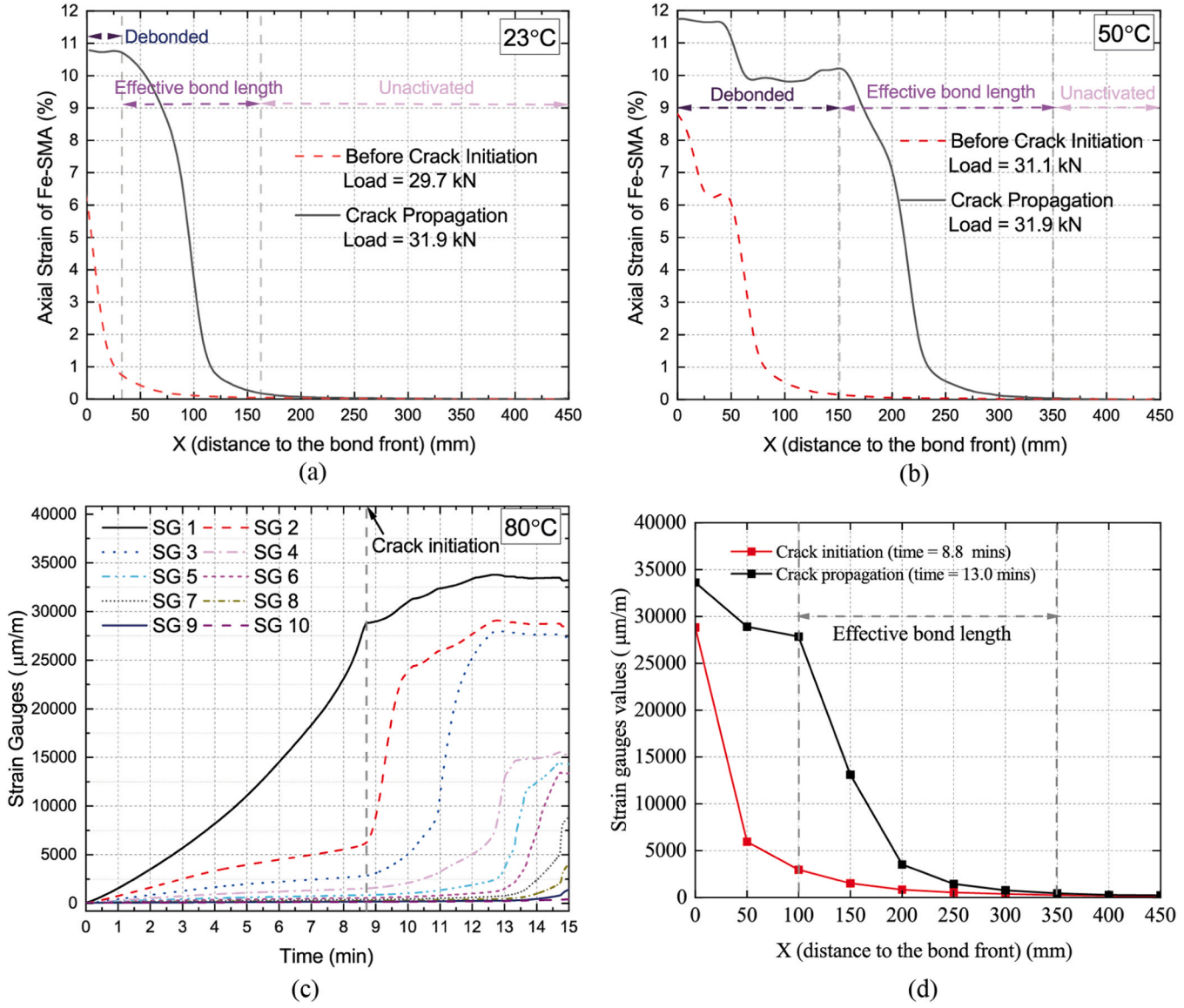

Fig. 15. Axial strain in the Fe-SMA at representative moments of a representative lap-shear test before crack initiation and during crack propagation at (a) 23 °C and (b) 50 °C, and strain development in the Fe-SMA strip of a representative lap-shear test at 80 °C (c), the strain gauges values along the bond line (d).

in Fig. 16d, represents the fracture energy G_f. It is a crucial property of adhesive joints and directly influences the bond capacity [40]. The specimens LS-03–23 °C and LS-06–50 °C had failure modes of Fe-SMA rupture and glass failure; hence, they were not considered for the investigations in this section. The specimen LS-09–80 °C was not included due to the accidental detachment of the LVDT during the test.

Fig. 17 illustrates the extent to which the peak shear stress and the fracture energy changed with temperature. The tests conducted at 23 °C, 50 °C, and 80 °C revealed average peak shear stresses of 18.0 MPa, 11.8 MPa, and 9.3 MPa, respectively. Since the failure modes were cohesive failures at 23 °C, the peak shear stress of 18.0 MPa at 23 °C indicated that the interfacial strength at this temperature exceeded this value. The failure modes were adhesive failures at 50 °C and 80 °C, which suggested that the shear strength of the adhesive was higher than the peak shear stresses of 11.8 MPa, and 9.3 MPa. A notable decrease in peak shear stress was observed with increasing temperatures. This trend was attributed to the adhesive becoming softer as the temperature increased, which facilitated a longer effective bond length. Consequently, the distribution of stress over this extended effective length resulted in lower peak shear stresses.

The fracture energies calculated for the tests at 23 °C, 50 °C, and 80 °C are shown in Fig. 17b. They are 14.6 MPa·mm, 14.2 MPa·mm, and 4.4 MPa·mm on average, respectively. The fracture energy only slightly decreased when the temperature increased from 23 °C to 50 °C, even though the shear strength decreased from 28 MPa at 23 °C to around 19 MPa at 50 °C [38]. This was due to the softening of the adhesive, which enabled a longer effective bond length. The slightly reduced fracture energy at 50 °C was the reason for the marginally reduced load-carrying capacity at 50 °C compared with that at 23 °C. The significantly lower fracture energy at 80 °C led to the significantly reduced load-carrying capacity at 80 °C.

4. Conclusions

The bond behaviour of Fe-SMA-to-glass lap-shear joints with a selected epoxy adhesive at 23 °C, 50 °C, and 80 °C were investigated in this study. The failure modes, the load-carrying capacity, the shear behaviour, the approximate effective bond length, and the fracture energy were investigated. The following conclusions could be obtained:

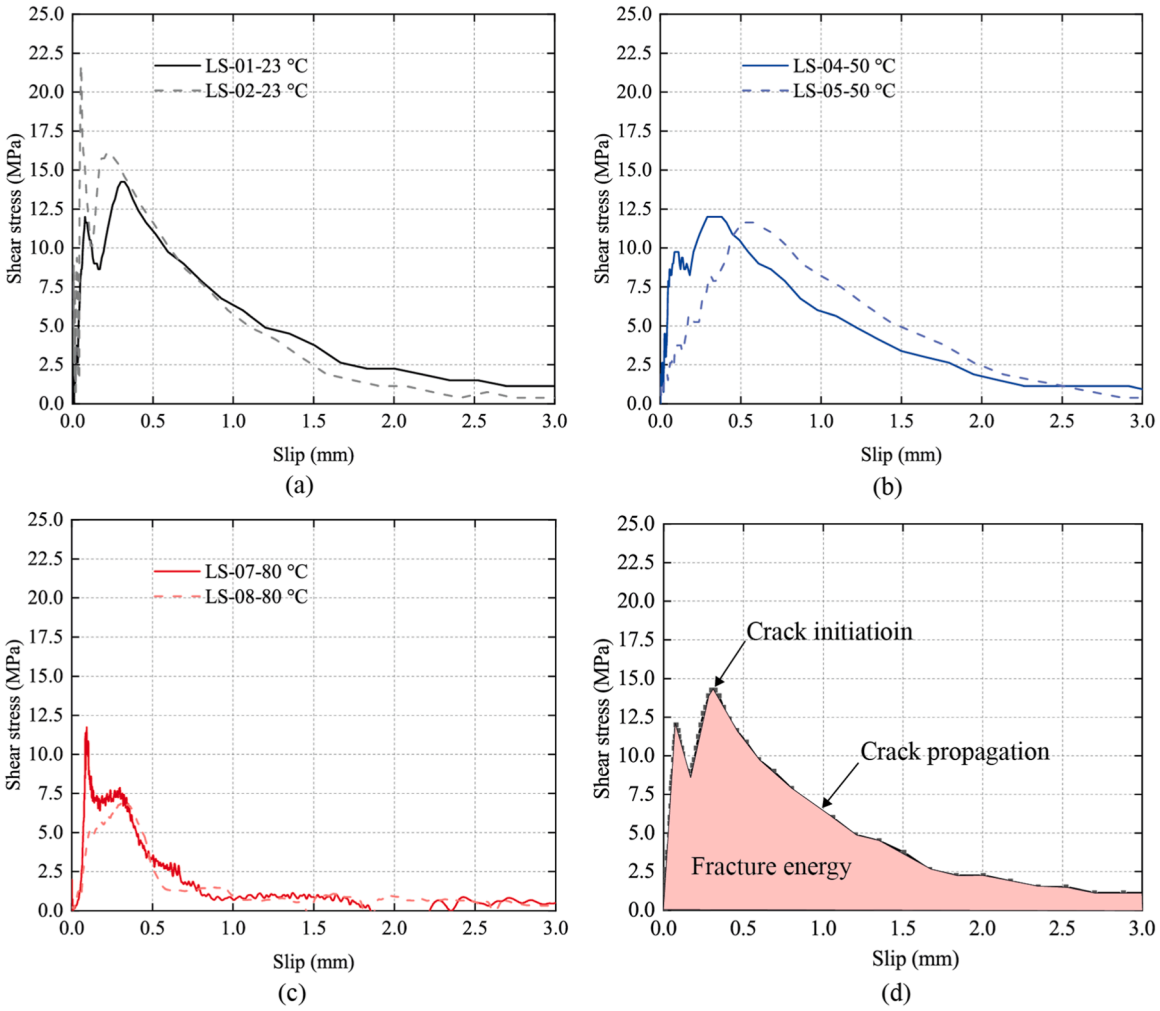

Fig. 16. Bond-slip behaviour of Fe-SMA-to-glass lap-shear tests at 23 °C (a), 50 °C (b), and 80 °C (c), and fracture energy at 23 °C (d).

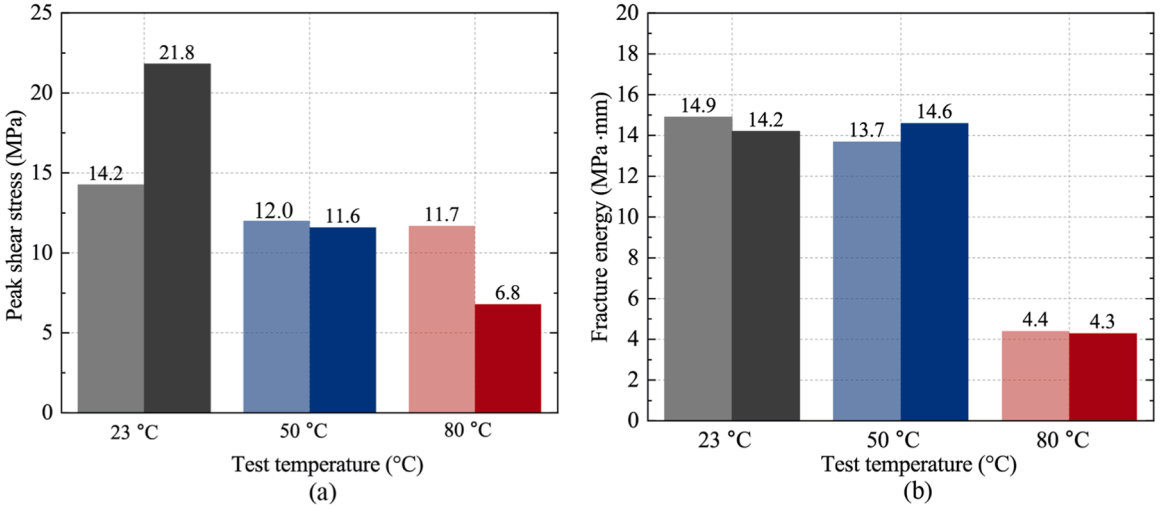

Fig. 17. Peak shear stress vs. temperature (a), and fracture energy vs. temperature (b).

- The major failure modes turned from cohesive failure at 23 °C to adhesive failure at elevated temperatures of 50 °C and 80 °C. The reason was the reduced interfacial strength at the elevated temperatures.
- Ductile failure modes could be achieved at 23 °C, 50 °C and 80 °C, however, the ductility was significantly lower at 80 °C compared with those at 23 °C and 50 °C.
- The crack initiation load and maximum load decreased by around 8.0 % and 8.4 %, respectively, when the temperature increased from

23 °C to 50 °C, while they decreased by around 17.8 % and 19.8 %, respectively, when the temperature increased from 23 °C to 80 °C.
- The effective bond length increased from 116 mm at 23 °C to 200 mm and 250–300 mm at 50 °C and 80 °C, respectively. This was due to the softening of the adhesive when the temperature increased.
- The fracture energy of 14.9 MPa at 23 °C was reduced to 14.2 MPa·mm at 50 °C and 4.4 MPa·mm at 80 °C. It resulted in reduced bond capacities at 50 °C and 80 °C, compared to that at 23 °C.

In addition to the aforementioned investigations of short-term behaviours at elevated temperatures, further studies should also explore the long-term effects of elevated temperatures, UV exposure, and humidity on the bonded joints between glass and Fe-SMA. Specifically, research should assess the bonding performance when Fe-SMA strips are bonded to the edges of glass beams. Additionally, it is crucial to develop effective simulation methods for designing post-tensioned glass beams under varying temperature conditions.

CRediT authorship contribution statement

Zhikang Deng: Writing – original draft, Visualization, Methodology, Investigation, Formal analysis, Data curation, Conceptualization. **Vlad-Alexandru Silvestru:** Writing – review & editing, Supervision, Methodology, Formal analysis. **Lingzhen Li:** Writing – review & editing, Methodology, Formal analysis, Data curation. **Elyas Ghafoori:** Writing – review & editing, Supervision, Methodology. **Andreas Taras:** Writing – review & editing, Supervision, Funding acquisition.

Declaration of Competing Interest

The authors declare that they have no known competing financial interests or personal relationships that could have appeared to influence the work reported in this paper.

Acknowledgements

The support of re-fer AG, Glas Trösch AG, AG INTERPANE Glasgesellschaft mbH, and Sika Schweiz AG with the materials necessary for the test specimens is gratefully acknowledged. Furthermore, the authors would like to thank the laboratory staff of the Institute of Structural Engineering at ETH Zurich (Dominik Werne, Andreas Reusser, Martin Viertel, Christoph Gisler, Thomas Jaggi, and Pius Herzog).

Data Availability

Data will be made available on request.

References

[1] J. Cupać, C. Louter, A. Nussbaumer, Flexural behaviour of post-tensioned glass beams: experimental and analytical study of three beam typologies, Compos. Struct. 255 (2021), https://doi.org/10.1016/j.compstruct.2020.112971.
[2] F. Firmo, S. Jordao, L.C. Neves, C. Bedon, Exploratory study on simple hybrid or pre-stressed steel-glass I-beams under short-term bending - Part 1: experiments, Compos. Struct. 234 (2020), https://doi.org/10.1016/j.compstruct.2019.111651.
[3] K. Martens, R. Caspeele, J.J.Jose Belis, Development of reinforced and post-tensioned glass beams: review of experimental research, J. Struct. Eng. 142 (5) (2016) 04015173, https://doi.org/10.1061/(ASCE)ST.1943-541X.0001453.
[4] J. Cupać, C. Louter, A. Nussbaumer, Exploring the potential of the critical shear crack theory for reinforced and post-tensioned glass beams: initial analysis and experiments, Eng. Struct. 279 (2023), https://doi.org/10.1016/j.engstruct.2022.115554.
[5] M. Achintha, B. Balan, Mechanical prestressing of annealed glass beams using pretensioned GFRP: characterisation and potentiality, Structures 20 (2019) 11–19, https://doi.org/10.1016/j.istruc.2019.02.017.
[6] C. Bedon, C. Louter, Numerical analysis of glass-FRP post-tensioned beams – review and assessment, Compos. Struct. 177 (2017) 129–140, https://doi.org/10.1016/j.compstruct.2017.06.060.
[7] J.M. Jani, M. Leary, A. Subic, Shape memory alloys in automotive applications, Appl. Mech. Mater. (2014).
[8] L. Lecce, Shape Memory Alloy Engineering: For Aerospace, Structural and Biomedical Applications. 2014.
[9] E. Ghafoori, B. Wang, B. Andrawes, Shape memory alloys for structural engineering: An editorial overview of research and future potentials, Eng. Struct. 273 (2022), https://doi.org/10.1016/j.engstruct.2022.115138.
[10] C. Czaderski, M. Shahverdi, E. Ghafoori, M. Motavalli, C. Leinenbach, A. Arabi-Hashemi, J. Michels, and J. Scherer. The development of memory steel at Empa, 5th International Conference on Smart Monitoring, Assessment and Rehabilitation of Civil Structures (SMAR), Potsdam. 2019.
[11] A. Cladera, B. Weber, C. Leinenbach, C. Czaderski, M. Shahverdi, M. Motavalli, Iron-based shape memory alloys for civil engineering structures: an overview, Constr. Build. Mater. 63 (2014) 281–293, https://doi.org/10.1016/j.conbuildmat.2014.04.032.
[12] E. Ghafoori, M. Neuenschwander, M. Shahverdi, C. Czaderski, M. Fontana, Elevated temperature behavior of an iron-based shape memory alloy used for prestressed strengthening of civil structures, Constr. Build. Mater. 211 (2019) 437–452, https://doi.org/10.1016/j.conbuildmat.2019.03.098.
[13] M. Shahverdi, J. Michels, C. Czaderski, M.J.C. Motavalli, and B. Materials, *Iron-based shape memory alloy strips for strengthening RC members: Material behavior and characterization.* 2018. **173**: p. 586-599. https://doi.org/10.1016/j.conbuildmat.2018.04.057.
[14] E. Fritsch, M. Izadi, and E. Ghafoori, *Nailed iron-based shape memory alloy (Fe-SMA) strips for strengthening of steel members*, in *5th International Conference on Smart Monitoring, Assessment and Rehabilitation of Civil Structures (SMAR), Potsdam*. 2019.
[15] E. Fritsch, M. Izadi, E. Ghafoori, Development of nail-anchor strengthening system with iron-based shape memory alloy (Fe-SMA) strips, Constr. Build. Mater. 229 (2019), https://doi.org/10.1016/j.conbuildmat.2019.117042.
[16] M.R. Izadi, E. Ghafoori, M. Shahverdi, M. Motavalli, S. Maalek, Development of an iron-based shape memory alloy (Fe-SMA) strengthening system for steel plates, Eng. Struct. 174 (2018) 433–446, https://doi.org/10.1016/j.engstruct.2018.07.073.
[17] V.A. Silvestru, Z. Deng, J. Michels, A. Taras, Enabling a ductile failure of laminated glass beams with iron-based shape memory alloy (Fe-SMA) Strips, SDSS 2022 (2022), https://doi.org/10.1002/cepa.1839.
[18] J. Rocha, E. Pereira, J. Sena-Cruz, Feasibility of mechanical post-tensioning of annealed glass beams by activating externally bonded Fe-SMA reinforcement, Constr. Build. Mater. 365 (2023), https://doi.org/10.1016/j.conbuildmat.2022.129953.
[19] V.A. Silvestru, Z. Deng, J. Michels, L. Li, E. Ghafoori, A. Taras, Application of an iron-based shape memory alloy for post-tensioning glass elements, Glass Struct. Eng. 7 (2022) 187–210, https://doi.org/10.1007/s40940-022-00183-z.
[20] J. Belis, A. Van Hulle, B. Out, F. Bos, D. Callewaert, and H.J.Po.G.P.D. Poulis, *Broad screening of adhesives for glass-metal bonds.* 2011: p. 286-289.
[21] M. Overend, Q. Jin, J. Watson, The selection and performance of adhesives for a steel–glass connection, Int. J. Adhes. Adhes. 31 (7) (2011) 587–597, https://doi.org/10.1016/j.ijadhadh.2011.06.001.
[22] I. Katsivalis, O.T. Thomsen, S. Feih, M. Achintha, Effect of elevated temperatures and humidity on glass/steel adhesive joints, Int. J. Adhes. Adhes. 102 (2020), https://doi.org/10.1016/j.ijadhadh.2020.102691.
[23] Z. Deng, V.-A. Silvestru, J. Michels, L. Li, E. Ghafoori, A. Taras, Performance of glass to iron-based shape memory alloy adhesive shear joints with different geometry, Challenging Glass Conf. Proc. 8 (2022), https://doi.org/10.47982/cgc.8.397.
[24] M. Yao, D. Zhu, Y. Yao, H. Zhang, B. Mobasher, Experimental study on basalt FRP/steel single-lap joints under different loading rates and temperatures, Compos. Struct. 145 (2016) 68–79, https://doi.org/10.1016/j.compstruct.2016.02.061.
[25] J. He, G. Xian, Y.X. Zhang, Effect of moderately elevated temperatures on bond behaviour of CFRP-to-steel bonded joints using different adhesives, Constr. Build. Mater. 241 (2020), https://doi.org/10.1016/j.conbuildmat.2020.118057.
[26] H. Zhou, D. Fernando, J.L. Torero, J.P. Torres, C. Maluk, R. Emberley, Bond behavior of CFRP-to-steel bonded joints at mild temperatures: experimental study, J. Compos. Constr. 24 (6) (2020), https://doi.org/10.1061/(asce)cc.1943-5614.0001073.
[27] H. Zhou, *Behaviour of FRP-to-concrete bonded joints under cyclic and thermal loading.* 2019.
[28] H. Zhou, W.-Y. Gao, H.C. Biscaia, X.-J. Wei, J.-G. Dai, Debonding analysis of FRP-to-concrete interfaces between two adjacent cracks in plated beams under temperature variations, Eng. Fract. Mech. 263 (2022) 108307, https://doi.org/10.1016/j.engfracmech.2022.108307.
[29] J.P. Firmo, J.R. Correia, D. Pitta, C. Tiago, M.R.T. Arruda, Experimental characterization of the bond between externally bonded reinforcement (EBR) CFRP strips and concrete at elevated temperatures, Cem. Concr. Compos. 60 (2015) 44–54, https://doi.org/10.1016/j.cemconcomp.2015.02.008.
[30] L. Li, E. Chatzi, C. Czaderski, E. Ghafoori, Influence of activation temperature and prestress on behavior of Fe-SMA bonded joints, Constr. Build. Mater. 409 (2023), https://doi.org/10.1016/j.conbuildmat.2023.134070.
[31] Z. Liu, Z. Dong, Y. Sun, H. Zhu, G. Wu, C. Sun, C.-K. Soh, Effect of resistive heating on the bond properties between iron-based shape memory bars and cement mortar, J. Build. Eng. 66 (2023), https://doi.org/10.1016/j.jobe.2023.105895.
[32] Z. Liu, P. Shi, H. Zhu, Z. Dong, W. Ning, G. Wu, Bond behavior between Fe-SMA strips and mortar in masonry joint after resistive heating, Constr. Build. Mater. 409 (2023), https://doi.org/10.1016/j.conbuildmat.2023.133871.
[33] ETAG 002, ETAG 002, Edition November 1999, Guideline for European technical approval for structural sealant glazing systems (SSGS), Part 1: Supported and unsupported systems. 1999.

[34] I. Katsivalis, O.T. Thomsen, S. Feih, M. Achintha, Development of cohesive zone models for the prediction of damage and failure of glass/steel adhesive joints, Int J. Adhes. Adhes. 97 (2020), https://doi.org/10.1016/j.ijadhadh.2019.102479.
[35] A. DIN, EN 572-1-2004. Glass in building. Part 1: Definitions and general physical and mechanical properties, 2004.
[36] L. Li, W. Wang, E. Chatzi, E. Ghafoori, Experimental investigation on debonding behavior of Fe-SMA-to-steel joints, Constr. Build. Mater. 364 (2023), https://doi.org/10.1016/j.conbuildmat.2022.129857.
[37] S. Wang, L. Li, Q. Su, X. Jiang, E. Ghafoori, Strengthening of steel beams with adhesively bonded memory-steel strips, Thin-Walled Struct. 189 (2023), https://doi.org/10.1016/j.tws.2023.110901.
[38] Sika, Additional product information material card SikaPower®-1277. 2021.
[39] V.-A. Silvestru, Z. Deng, A. Taras, On predicting the behaviour of an iron-based shape memory alloy with the Ramberg-Osgood model, Eurosteel 2023 (2023), https://doi.org/10.1002/cepa.2383.
[40] L. Li, E. Chatzi, E. Ghafoori, Debonding model for nonlinear Fe-SMA strips bonded with nonlinear adhesives, Eng. Fract. Mech. 282 (2023) 109201, https://doi.org/10.1016/j.engfracmech.2023.109201.